arXiv:1608.05800v1 [cond-mat.mtrl-sci] 20 Aug 2016

Thermoelectric properties of topological insulator $BaSn_2$

San-Dong Guo and Liang Qiu
Department of Physics, School of Sciences, China University of Mining and Technology, Xuzhou 221116, Jiangsu, China

Recently, $BaSn_2$ is predicted to be a strong topological insulator by the first-principle calculations. It is well known that topological insulator has a close connection to thermoelectric material, such as Bi_2Te_3 family. In this work, we investigate thermoelectric properties of $BaSn_2$ by the first-principles combined with Boltzmann transport theory. The electronic part is carried out by a modified Becke and Johnson (mBJ) exchange potential, including spin-orbit coupling (SOC), while the phonon part is performed using generalized gradient approximation (GGA). It is found that the electronic transport coefficients between the in-plane and cross-plane directions show the strong anisotropy, while lattice lattice thermal conductivities show an almost isotropy. Calculated results show a very low lattice thermal conductivity for $BaSn_2$, and the corresponding average lattice thermal conductivity at room temperature is 1.69 $Wm^{-1}K^{-1}$, which is comparable or lower than those of lead chalcogenides and bismuth-tellurium systems as classic thermoelectric materials. Due to the complicated scattering mechanism, calculating scattering time τ is challenging. By using a empirical τ=10^{-14} s, the n-type figure of merit ZT is greater than 0.40 in wide temperature range. Experimentally, it is possible to attain better thermoelectric performance, or to enhance one by strain or tuning size parameter. This work indicates that $BaSn_2$ may be a potential thermoelectric material, which can stimulate further theoretical and experimental works.

PACS numbers: 72.15.Jf, 71.20.-b, 71.70.Ej, 79.10.-n
Keywords: Topological insulator; Power factor; Thermal conductivity

I. INTRODUCTION

Searching high-performance thermoelectric materials is challenging and urgent, which can make essential contributions to energy crisis and global warming by directly converting heat to electricity. The dimensionless thermoelectric figure of merit ZT, which determines the performance of thermoelectric material[1,2], can be written as

$$ZT = S^2\sigma T/(\kappa_e + \kappa_L) \quad (1)$$

where S, σ, T, κ_e and κ_L are the Seebeck coefficient, electrical conductivity, absolute working temperature, the electronic and lattice thermal conductivities, respectively. To attain a high ZT, a high power factor ($S^2\sigma$) and a low thermal conductivity ($\kappa = \kappa_e + \kappa_L$) are required. Unfortunately, Seebeck coefficient and electrical conductivity are generally coupled with each other, and they are oppositely proportional to carrier density. So, an appropriate carrier density, neither too big nor too small, can lead to the maximum power factor, and then narrow band-gap materials are potential for efficient thermoelectric applications[3]. Topological insulators, characterized by a full insulating bulk gap and gapless edge states[4,5], share similar material properties with thermoelectric materials, such as heavy elements and narrow gaps. For example bismuth-tellurium systems, they are both famous topological insulators[6] and good thermoelectric materials[7]. It has been demonstrated that ZT of topological insulators is strongly size dependent, and can be improved to be greater than 1 by tuning size parameter[8].

Recently, $BaSn_2$ has been predicted to be a new strong topological insulator[9,10], which is composed of alternating buckled honeycomb Sn layers and flat triangular Ba layers. A topological band inversion is at high symmetry A point, which is different from known strong topological insulators inverting at high symmetry Γ point. It is interesting and urgent to investigate thermoelectric properties of $BaSn_2$. Another important cause is that $BaSn_2$ contains buckled honeycomb Sn layers known as stanene, which has been realized via molecular beam epitaxy on a Bi_2Te_3 substrate[11]. Stanene with buckled honeycomb structure like silicene[12] and germanene[13] has been also predicted to be a topological insulator, supporting a large-gap two-dimensional (2D) quantum spin Hall state[14]. The thermoelectric properties of Stanene also have been investigated[8,15], and the corresponding room-temperature lattice thermal conductivity is 11.6 $Wm^{-1}K^{-1}$[15]. It is also interesting to know whether Ba layers can produce reduced effects on lattice thermal conductivity.

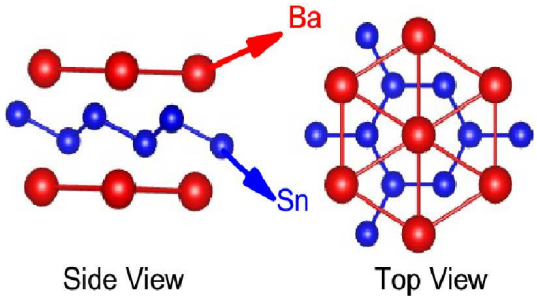

FIG. 1. The crystal structures of $BaSn_2$, which is composed of alternating buckled honeycomb Sn layers and flat triangular Ba layers.

Here, we investigate the thermoelectric properties of $BaSn_2$, including both electron and phonon parts. Cal-

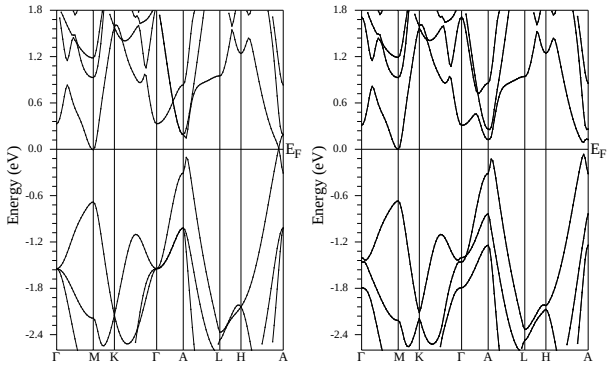

FIG. 2. The energy band structures of $BaSn_2$ using mBJ (Left) and mBJ+SOC (Right).

culated results show that the electronic transport coefficients along a and c axises show the strong anisotropy. At room temperature, the lattice thermal conductivity is 1.77 $Wm^{-1}K^{-1}$ along a axis and 1.54 $Wm^{-1}K^{-1}$ along c axis, respectively, which is lower than one (11.6 $Wm^{-1}K^{-1}$) of Stanene, and which is also comparable or lower than those of good thermoelectric materials, such as lead chalcogenides and bismuth-tellurium systems. The additional result is that the structural stability of $BaSn_2$ is proved by phonon dispersion and mechanical stability criterion within elastic constants. According to calculated ZT values, it is found that n-type doping may provide better thermoelectric performance.

The rest of the paper is organized as follows. In the next section, we shall describe computational details for first-principle and transport coefficients calculations. In the third section, we shall present the electronic structures and thermoelectric properties of $BaSn_2$. Finally, we shall give our discussions and conclusion in the fourth section.

II. COMPUTATIONAL DETAIL

A full-potential linearized augmented-plane-waves method within the density functional theory (DFT)[16] is employed to study electronic structures of $BaSn_2$, as implemented in the package WIEN2k[17]. An improved Tran and Blaha's mBJ exchange potential plus local-density approximation (LDA) correlation potential for the exchange-correlation potential[18] is employed to produce more accurate band gaps. The free atomic position parameters are optimized using GGA of Perdew, Burke and Ernzerhof (GGA-PBE)[19] with a force standard of 2 mRy/a.u.. The full relativistic effects are calculated with the Dirac equations for core states, and the scalar relativistic approximation is used for valence states[20–22]. The SOC was included self-consistently by solving the radial Dirac equation for the core electrons and evaluated by the second-variation method[23]. The convergence results are determined by using 6000 k-points in the first Brillouin zone for the self-consistent calculation, making harmonic expansion up to $l_{max} = 10$ in each of the atomic spheres, and setting $R_{mt} * k_{max} = 8$ for the plane-wave cut-off. The self-consistent calculations are considered to be converged when the integration of the absolute charge-density difference between the input and output electron density is less than $0.0001|e|$ per formula unit, where e is the electron charge. Based on the results of electronic structure, transport coefficients for electron part are calculated through solving Boltzmann transport equations within the constant scattering time approximation (CSTA), as implemented in BoltzTrap[24], which shows reliable results in many classic thermoelectric materials[25–27]. To obtain accurate transport coefficients, we set the parameter LPFAC for 10, and use 32000 k-points (35×35×25 k-point mesh) in the first Brillouin zone for the energy band calculation. The lattice thermal conductivities are performed by using Phono3py+VASP codes[28–31]. For the third-order force constants, 2×2×2 supercells are built, and reciprocal spaces of the supercells are sampled by 4×4×3 meshes. To compute lattice thermal conductivities, the reciprocal spaces of the primitive cells are sampled using the 20×20×19 meshes.

TABLE I. Lattice thermal conductivities (Unit:$Wm^{-1}K^{-1}$) of $BaSn_2$, lead chalcogenides[42] and bismuth-tellurium systems[43,44] at 300 K.

$BaSn_2$	PbS	PbSe	PbTe	Bi_2Te_3	Sb_2Te_3	Bi_2Se_3
1.69	2.9	2.0	2.5	1.6	2.4	1.34

III. MAIN CALCULATED RESULTS AND ANALYSIS

$BaSn_2$ crystallizes in the $EuGe_2$-type hexagonal structure with space group being $P\bar{3}m1$ (No.164), which is composed of alternating buckled honeycomb Sn layers and flat triangular Ba layers (See Figure 1). According to stacking of Sn, the Sn layer is actually famous stanene[11], a monolayer with buckled honeycomb structure like silicene and germanene[12,13]. In our calculations, the experimental values (a=b=4.652 Å, c=5.546 Å)[32] are used for a, b and c, and the free atomic position of Sn is optimized within GGA-PBE. The optimized position of Sn (1/3, 2/3, 0.107) is in good agreement with experimental value of Sn (1/3, 2/3, 0.103). An improved mBJ exchange potential is employed to investigate electronic structures of $BaSn_2$, which is superior to GGA and LDA for gap calculations. $BaSn_2$ is predicted to be a topological insulator[9,10], so SOC is included for electron part. The energy band structures of $BaSn_2$ using both mBJ and mBJ+SOC are plotted Figure 2. It is found that SOC has observable effects on energy bands around high symmetry A point. The mBJ results show that the valence band extrema (VBE) and conduction band extrema (CBE) along H-A line almost coincide,

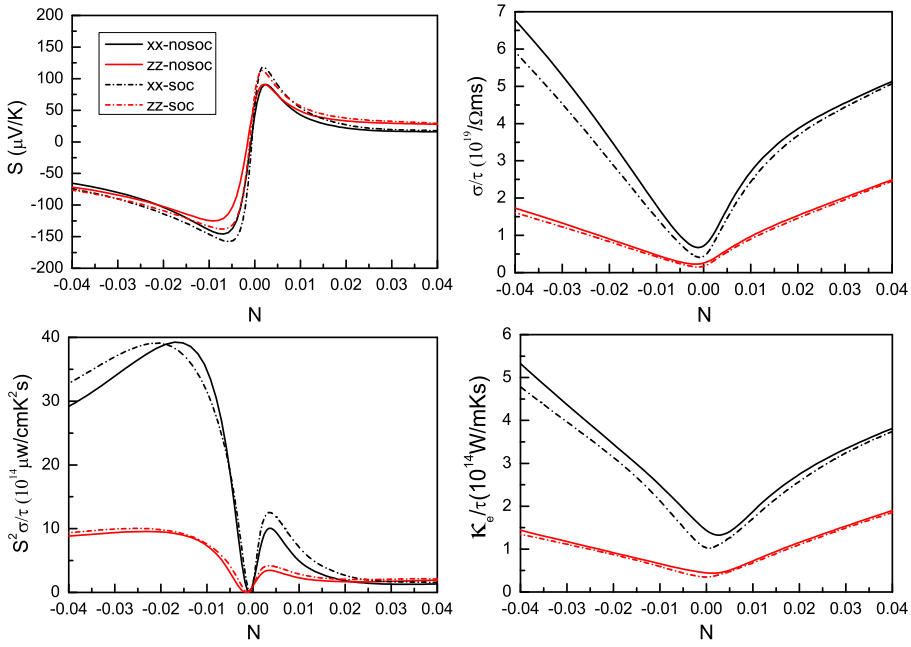

FIG. 3. (Color online) At room temperature (300 K), transport coefficients as a function of doping level (N) along a and c axises: Seebeck coefficient S, electrical conductivity with respect to scattering time σ/τ, power factor with respect to scattering time $S^2\sigma/\tau$ and electronic thermal conductivity with respect to scattering time κ_e/τ calculated with mBJ and mBJ+SOC.

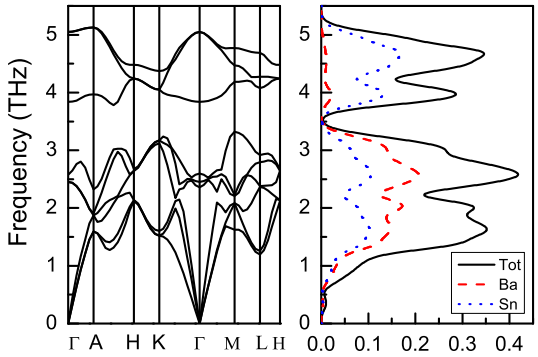

FIG. 4. Phonon band structure with phonon DOS of $BaSn_2$ using GGA-PBE.

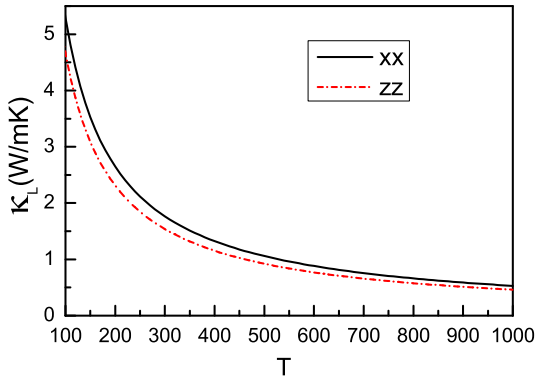

FIG. 5. The lattice thermal conductivities of $BaSn_2$ along a and c axises using GGA-PBE.

while a gap of 156 meV is produced with mBJ+SOC. Another noteworthy thing is that $BaSn_2$ has many CBE with their energies being very close, which is benefit for high Seebeck coefficient[1].

The transport coefficients for electron part, including Seebeck coefficient and electrical conductivity, are carried out using CSTA Boltzmann theory. Seebeck coefficient is independent of scattering time, while electrical conductivity depends on scattering time. Within the framework of rigid band approach, the doping level can be achieved by simply shifting Fermi level, which is reasonable in the low doping level in many thermoelectric materials[33–35]. The doping level is defined as electrons (minus value) or holes (positive value) per unit cell. The n-type doping (negative doping levels) can be simulated by shifting Fermi level into conduction bands, producing the negative Seebeck coefficient. When the Fermi level moves into valence bands, the p-type doping (positive doping levels) with the positive Seebeck coefficient can be achieved.

Due to crystal symmetry of $BaSn_2$, the physical properties along a and b axises (the in-plane direction) are equivalent, which are different from those along c axis (the cross-plane direction), so we only show transport coefficients along a and c axises. At 300 K, the doping level dependence of Seebeck coefficient S, electrical conductivity with respect to scattering time σ/τ, power factor with respect to scattering time $S^2\sigma/\tau$ and electrical thermal conductivity with respect to scattering time κ_e/τ along a and c axises using mBJ and mBJ+SOC are plotted in Figure 3. It is found that SOC has a enhanced effect on Seebeck coefficient, which can be explained by

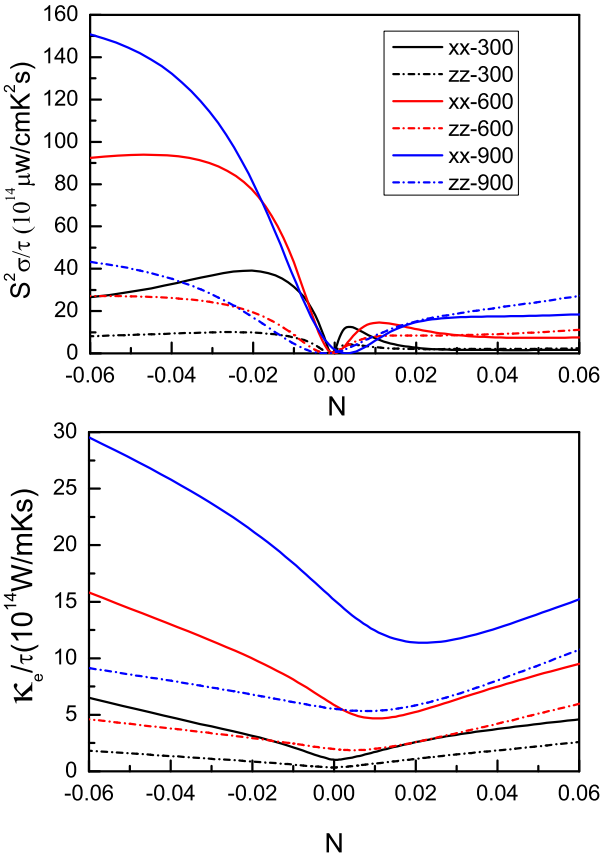

FIG. 6. The power factor with respect to scattering time $S^2\sigma/\tau$ and electronic thermal conductivity with respect to scattering time κ_e/τ along a and c axises as a function of doping level with temperature being 300, 600 and 900 K.

that some VBE or CBE are more close to each other at the presence of SOC. But, SOC has a reduced influence on electrical conductivity and electrical thermal conductivity. Calculated results show that SOC has a mildly improved effect on power factor, except for n-type one along a axis in low doping. The n-type doping has larger Seebeck coefficient than the p-type one, which is because the numbers of CBE with adjacent energy are more than ones of VBE, and then n-type power factor is very larger than p-type one. The anisotropy of Seebeck coefficient along a and c axises is tiny, while electrical conductivity shows strong anisotropy. The electrical conductivity along a axis is almost three times as large as one along c axis, which implies the in-plane direction as a much more conductive direction. The power factor and electrical thermal conductivity show the same anisotropy with electrical conductivity. It is observed that electrical thermal conductivity has similar trend with electrical conductivity, which is due to the Wiedemann-Franz law: $\kappa_e = L\sigma T$, where L is the Lorenz number.

The phonon band structure with phonon density of states (DOS) of $BaSn_2$ using GGA-PBE are shown in Figure 4. The unit cell of $BaSn_2$ contains two Sn and one Ba atoms, resulting in 3 acoustic and 6 optical phonon branches. The maximum optical frequency of 5.13 THz is comparable with the corresponding values of good thermoelectric materials, such as Bi_2Te_3[36] (4.5 THz) and SnSe[37] (5.6 THz). The maximal acoustic vibration frequency in $BaSn_2$ is only 2.36 THz, which is benefit to low thermal conductivity. It is found that the phonon dispersions are separated into two regions with a gap around 0.47 THz. According to projected DOS in Ba and Sn atoms, it can be noted that the lower (upper) part of phonon dispersions mainly is due to the vibrations of the heavy Ba (light Sn) atoms. Calculated results show that no imaginary frequency modes are produced, suggesting no structural instability at low temperature for $BaSn_2$.

Based on the following mechanical stability criterion for a rhombohedral structure[38]:

$$C_{11} - |C_{12}| > 0 \tag{2}$$

$$(C_{11} + C_{12})C_{33} - 2C_{13}^2 > 0 \tag{3}$$

$$(C_{11} - C_{12})C_{44} - 2C_{14}^2 > 0 \tag{4}$$

The C_{ij} are five independent elastic constants, and the calculated values are listed in Table II. It is easy to conclude that these criteria are satisfied for $BaSn_2$, implying mechanical stability of $BaSn_2$. Based on calculated elastic constants C_{ij}, the bulk modulus B, shear modulus G, Young's modulus E_x and E_z can be attained, and list them in Table II. B/G can measure ductility and brittleness, and the critical value separating ductile and brittle materials is ∼1.75[38]. The calculated ratio is 1.89, indicating the ductile nature of $BaSn_2$. The anisotropy ratios also can be calculated by the following expressions:

$$A_1 = 2C_{44}/(C_{11} - C_{12}) \tag{5}$$

$$A_2 = 4C_{44}/(C_{11} + C_{33} - 2C_{13}) \tag{6}$$

The numeric values of A_1 and A_2 are 1.39 and 1.64, which are close to unity, suggesting relatively small anisotropy. The related data are also summarized in Table II. Moreover, it is very interesting that the elastic parameters of $BaSn_2$ are very close to ones of good thermoelectric material Bi_2Te_3[39], which may mean they share similar lattice thermal conductivity.

TABLE II. The calculated elastic constants C_{ij} , bulk modulus B , shear modulus G and Young's modulus E_x, E_y (Their Unit: GPa); B/G and anisotropy factor A_1, A_2.

C_{11}	C_{12}	C_{13}	C_{14}	C_{33}	C_{44}	B
71.89	31.81	23.39	12.46	43.10	27.91	36.63
G	E_x	E_z	B/G	A_1	A_2	
19.39	42.28	32.55	1.89	1.39	1.64	

TABLE III. Peak ZT along a and c axises for both n- and p-type with τ=10^{-14} s, and the corresponding doping concentrations. The doping concentration equals 9.621 × 10^{21}cm^{-3} × doping level.

	a-axis				c-axis			
	n		p		n		p	
T (K)	(×10^{19}cm^{-3})	ZT	(×10^{19}cm^{-3})	ZT	(×10^{19}cm^{-3})	ZT	(×10^{19}cm^{-3})	ZT
300	13.99	0.25	3.26	0.13	17.53	0.12	3.26	0.06
600	25.32	0.44	10.55	0.16	31.93	0.35	10.55	0.17
900	45.99	0.46	28.58	0.13	57.49	0.40	29.75	0.23

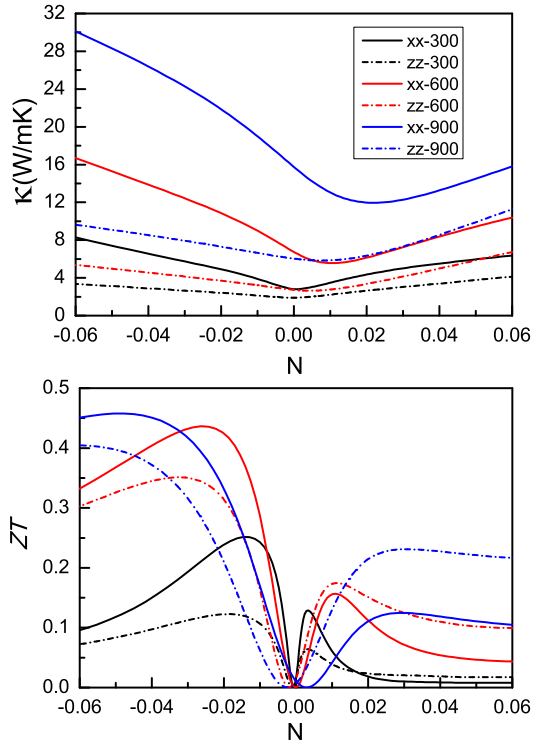

FIG. 7. The thermal conductivity κ=κ_e+κ_L and ZT along a and c axises as a function of doping level with temperature being 300, 600 and 900 K, and the scattering time τ equals 1 × 10^{-14} s.

Based on harmonic and anharmonic interatomic force constants, the lattice thermal conductivities of $BaSn_2$ can be obtained, which along a and c axises as a function of temperature are plotted Figure 5. It is assumed that the lattice thermal conductivity is independent of doping level, and typically goes as 1/T, which can be found in many thermoelectric materials[40,41]. It is found that the lattice thermal conductivity exhibits little anisotropy, where the lattice thermal conductivity along c axis is lower than that along a axis. The room-temperature lattice thermal conductivity is 1.77 Wm^{-1}K^{-1} along a axis and 1.54 Wm^{-1}K^{-1} along c axis, respectively, which is very lower than that of (11.6 Wm^{-1}K^{-1}) of Stanene[15] due to Ba layers. The average lattice thermal conductivity 1.69 Wm^{-1}K^{-1} along three axises can match with ones of lead chalcogenides and bismuth-tellurium systems as classic thermoelectric materials[42–44], and we summary related lattice thermal conductivities in Table I. The lattice thermal conductivity of $BaSn_2$ is even lower than ones of conventional good thermoelectric materials except for Bi_2Se_3 and Bi_2Te_3. Such a low lattice thermal conductivity implies $BaSn_2$ may be a potential thermoelectric material.

Finally, we consider possible efficiency of thermoelectric conversion based on calculated transport coefficients of electron and phonon parts. The power factor and electronic thermal conductivity with respect to scattering time $S^2\sigma/\tau$ and κ_e/τ along a and c axises as a function of doping level with temperature being 300, 600 and 900 K are plotted in Figure 6. To attain the figure of merit ZT, a unknown parameter is scattering time τ. Calculating scattering time τ from the first-principle calculations is difficulty because of the complexity of various carrier scattering mechanisms. If some experimental transport coefficients are available, the scattering time can be attained by comparing the experimental transport coefficients with calculated ones, such as electrical conductivity. Unfortunately, the related experimental transport coefficients of $BaSn_2$ are unavailable, and we use a empirical scattering time 1 × 10^{-14} s to estimate possible ZT values. The thermal conductivity κ=κ_e+κ_L and ZT along a and c axises as a function of doping level with temperature being 300, 600 and 900 K are shown in Figure 7. In n-type doping, the figure of merit along a axis is always larger than the figure of merit along c axis. In p-type doping, the a-axis figure of merit is larger than the c-axis figure of merit at low temperature, and c-axis figure of merit becomes more larger with the increasing temperature. It is found that n-type doping exhibits more superior thermoelectric performance than p-type doping due to more higher n-type power factor. The peak ZT along a and c axises and corresponding doping concentrations at three different temperatures for both n- and p-type are shown in Table III. It is found that doping concentration of peak ZT increases with increasing temperature. In n-type doping, at 900 K, the a-axis ZT is as high as 0.46, and 0.40 for c-axis ZT. These results make us believe that $BaSn_2$ may be a potential thermoelectric material.

IV. DISCUSSIONS AND CONCLUSION

As is well known, energy band gap produces important effects on transport coefficients for electron part. Narrow gap with high carrier mobility favours the high electrical conductivity[45], but gapless behavior leads to a vanishing Seebeck coefficient[46]. Seebeck coefficient and electrical conductivity are oppositely proportional to carrier density. The electronic thermal conductivity is proportional to electrical conductivity by Wiedemann-Franz law. An upper limit of ZT can be expressed as $ZT_e = S^2\sigma T/\kappa_e$, neglecting lattice thermal conductivity. So, an appropriate energy band gap is needed to attain high ZT_e, like Bi_2Te_3 (0.15 eV)[47], but the mBJ+SOC gap of $BaSn_2$ is only 0.065 eV. At 300 K, the best n-type Seebeck coefficient (about 150 μV/K) is very weaker than p-type one (about 300 μV/K) and n-type one (about 250 μV/K) of Bi_2Te_3[47], due to too small energy band gap. However, narrow energy band gap induces high electrical conductivity for $BaSn_2$, which also indicates high electronic thermal conductivity. Due to high electrical conductivity, the average best n-type power factor (about $25\times10^{14}\mu$W/cmK^{2}s) of $BaSn_2$ is larger than best p-type one (about $15\times10^{14}\mu$W/cmK^{2}s) of Bi_2Te_3 at room temeperature[47]. In spite of higher power factor, the average best n-type ZT_e (about 0.42) is lower than best p-type one (about 0.70) of Bi_2Te_3 at 300 K[48], because of higher electronic thermal conductivity.

For gap calculations, mBJ is usually superior to GGA or LDA, but it may still underestimate the energy band gap of $BaSn_2$. So, $BaSn_2$ may have better thermoelectric performance. The energy band gap also can be tuned by strain. For example LaPtBi[48], when a stretched uniaxial strain is applied, it changes from semimetal into real topological insulator, achieving comparable thermoelectric performance with Bi_2Te_3 by an 8% stretched uniaxial strain. It is possible for $BaSn_2$ to achieve enhanced thermoelectric performance by strain. In ref.[8], Xu et al. point out that ZT is no longer an intrinsic material property in topological insulator, but is strongly size dependent. Tuning size parameter can dramatically increase ZT, being significantly greater than 1. Here, we have ignored the gapless edge states contribution to conducting channels, which helps to great improvement of thermoelectric performance by tuning size parameter. Experimentally, it is possible to achieve further enhanced thermoelectric performance of $BaSn_2$ by tuning size parameter.

In summary, the thermoelectric properties of $BaSn_2$, including both electron and phonon parts, are investigated based mainly on the reliable first-principle calculations. It is found that SOC has little influence on electronic transport coefficients. Calculated results show obvious anisotropy of power factor and electronic thermal conductivity between the in-plane and cross-plane directions, while a slight anisotropy of lattice thermal conductivity is observed. The low lattice thermal conductivity is predicted, and the average one is 1.69 Wm^{-1}K^{-1} at room temperature, which highlights possibility for $BaSn_2$ as a potential thermoelectric material. From 600 K to 900 K, the n-type figure of merit ZT is up to about 0.45 with empirical τ=10^{-14} s by optimizing doping level, and it is possible to achieve improved thermoelectric performance by strain and tuning size parameter in experiment. The present work may be useful to encourage further theoretical and experimental efforts to achieve high thermoelectric performance of $BaSn_2$.

ACKNOWLEDGMENTS

This work is supported by the Fundamental Research Funds for the Central Universities (2015QNA44). We are grateful to the Advanced Analysis and Computation Center of CUMT for the award of CPU hours to accomplish this work.

[1] Y. Pei, X. Shi, A. LaLonde, H. Wang, L. Chen and G. J. Snyder, Nature **473**, 66 (2011).
[2] L. E. Bell, Science **321**, 1457 (2008).
[3] G. J. Snyder and E. S. Toberer, Nat. Mater. **7**, 105 (2008).
[4] M. Z. Hasan and C. L. Kane, Rev. Mod. Phys. **82**, 3045 (2010).
[5] X. L. Qi and S. C. Zhang, Rev. Mod. Phys. **83**, 1057 (2011).
[6] H. J. Zhang, C. X. Liu, X. L. Qi, X. Dai, Z. Fang, and S. C. Zhang, Nat. Phys. **5**, 438 (2009).
[7] D. K. Ko, Y. J. Kang and C. B. Murray, Nano Lett. **11**, 2841 (2011).
[8] Y. Xu, Z. Gan, and S. C. Zhang, Phys. Rev. Lett. **112**, 226801 (2014).
[9] S. M. Young, J. P. Shao and A. N. Kolmogorov, arXiv:1607.05234 (2016).
[10] J. P. Shao, C. Beaufils and A. N. Kolmogorov, Sci. Rep. **6**, 28369 (2016).
[11] F. F. Zhu et al. Nat Mater **14**, 1020 (2015).
[12] H. I. T. Hauge et al. Nano Letters **15**, 5855 (2015).
[13] M. E. Dávila et al. New Journal of Physics **16**, 095002 (2014).
[14] Y. Xu et al. Phys. Rev. Lett. **111**, 136804 (2013).
[15] B. Peng et al. Sci. Rep. **6**, 20225 (2016).
[16] P. Hohenberg and W. Kohn, Phys. Rev. **136**, B864 (1964); W. Kohn and L. J. Sham, Phys. Rev. **140**, A1133 (1965).
[17] P. Blaha, K. Schwarz, G. K. H. Madsen, D. Kvasnicka and J. Luitz, WIEN2k, an Augmented Plane Wave + Local Orbitals Program for Calculating Crystal Properties (Karlheinz Schwarz Technische Universität Wien, Austria) 2001, ISBN 3-9501031-1-2
[18] F. Tran and P. Blaha, Phys. Rev. Lett. **102**, 226401 (2009).
[19] J. P. Perdew, K. Burke and M. Ernzerhof, Phys. Rev. Lett. **77**, 3865 (1996).
[20] A. H. MacDonald, W. E. Pickett and D. D. Koelling, J.

Phys. C **13**, 2675 (1980).
[21] D. J. Singh and L. Nordstrom, Plane Waves, Pseudopotentials and the LAPW Method, 2nd Edition (Springer, New York, 2006).
[22] J. Kunes, P. Novak, R. Schmid, P. Blaha and K. Schwarz, Phys. Rev. B **64**, 153102 (2001).
[23] D. D. Koelling, B. N. Harmon, J. Phys. C Solid State Phys. **10**, 3107 (1977).
[24] G. K. H. Madsen and D. J. Singh, Comput. Phys. Commun. **175**, 67 (2006).
[25] B. L. Huang and M. Kaviany, Phys. Rev. B **77**, 125209 (2008).
[26] L. Q. Xu, Y. P. Zheng and J. C. Zheng, Phys. Rev. B **82**, 195102 (2010).
[27] J. J. Pulikkotil, D. J. Singh, S. Auluck, M. Saravanan, D. K. Misra, A. Dhar and R. C. Budhani, Phys. Rev. B **86**, 155204 (2012).
[28] G. Kresse, J. Non-Cryst. Solids **193**, 222 (1995).
[29] G. Kresse and J. Furthm*ü*ller, Comput. Mater. Sci. 6, **15** (1996).
[30] G. Kresse and D. Joubert, Phys. Rev. B **59**, 1758 (1999).
[31] A. Togo, L. Chaput and I. Tanaka, Phys. Rev. B **91**, 094306 (2015).
[32] The experimental crystal structure is attained from the Inorganic Crystal Structure Database (ICSD).
[33] T. J. Scheidemantel, C. Ambrosch-Draxl, T. Thonhauser, J. V. Badding and J. O. Sofo, Phys. Rev. B **68**, 125210 (2003).
[34] G. K. H. Madsen, J. Am. Chem. Soc. **128**, 12140 (2006).
[35] X. Gao, K. Uehara, D. Klug, S. Patchkovskii, J. Tse and T. Tritt, Phys. Rev. B **72**, 125202 (2005).
[36] B. Qiu and X. Ruan, Phys. Rev. B **80**, 165203 (2009).
[37] J. Carrete, N. Mingo, and S. Curtarolo, Appl. Phys. Lett. **105**, 101907 (2014).
[38] S. L. Shang, G. Sheng, Y. Wang, L. Q. Chen and Z. K. Liu, Phys. Rev. B **80**, 052102 (2009).
[39] B. L. Huang and M. Kaviany, Phys. Rev. B **77**, 125209 (2008).
[40] D. Parker and D. J. Singh, Phys. Rev. B **82**, 035204 (2010).
[41] J. J. Pulikkotil et al., Phys. Rev. B **86**, 155204 (2012).
[42] D. T. Morelli and G. A. Slack, in High Thermal Conductivity Materials, edited by S. L. Shind*é* and J. S. Goela (Springer, New York, 2006).
[43] E. S. Toberer, A. Zevalkink, and G. J. Snyder, J. Mater. Chem. **21**, 15843 (2011).
[44] Springer Materials: The Landolt-B*ö*rnstein Database, http://www.springermaterials.com/docs/index.html
[45] M*ü*chler, F. Casper, B. Yan, S. Chadov, and C. Felser, Phys. Status Solidi RRL **7**, 91 (2013).
[46] D. I. Bilc and P. Ghosez, Phys. Rev. B **83**, 205204 (2011).
[47] H. Shi, D. Parker, M. H. Du, and D. J. Singh, Phys. Rev. Appl. **3**, 014004 (2015).
[48] G. Q. Ding, G. Y. Gao, L. Yu, Y. Ni and K. L. Yao, J. Appl. Phys. **119**, 025105 (2016).